Electrochemistry Communications 136 (2022) 107239

Contents lists available at ScienceDirect

Electrochemistry Communications

journal homepage: www.elsevier.com/locate/elecom

Full Communication

Hydrogen peroxide generation catalyzed by battery waste material

Magdalena Warczak [a,*], Magdalena Osial [b,c], Weronika Urbanska [d], Marcin Pisarek [a], Wojciech Nogala [a], Marcin Opallo [a,*]

[a] Institute of Physical Chemistry, Polish Academy of Sciences, Warsaw, Poland
[b] Faculty of Chemistry, University of Warsaw, Warsaw, Poland
[c] Department of Theory of Continuous Media and Nanostructures, Institute of the Fundamental Technological Research, Polish Academy of Sciences, Warsaw, Poland
[d] Faculty of Environmental Engineering, Wroclaw University of Science and Technology, Wroclaw, Poland

ARTICLE INFO

Keywords:
Hydrogen peroxide
Lithium-ion battery waste
Oxygen reduction
Scanning electrochemical microscopy (SECM)
Liquid–liquid interface

ABSTRACT

Lithium-ion battery (LiB) waste powder is a valuable source of various materials, including carbon and metals. Although this material exhibits electrical conductivity, nanostructured morphology, and may contain metal oxides, it has not been used as an electrocatalyst. Here, we demonstrated the application of LiB waste powder as a catalyst for electrochemical H_2O_2 generation. The powder was both immobilized on a glassy carbon (GC) electrode and assembled at a liquid–liquid interface formed by decamethylferrocene (DMFc) solution in trifluorotoluene and aqueous perchloric acid in the presence of oxygen. The electrochemistry was studied by cyclic voltammetry and also with a rotating disk electrode (RDE), and a 2-electron ORR pathway was confirmed. H_2O_2 generation at the liquid–liquid interface and oxidation of DMFc were detected by colorimetry, UV–vis spectroscopy and scanning electrochemical microscopy (SECM). The use of LiB waste powder reduces the ORR onset potential by ca. 0.3 V compared to an unmodified GC. When assembled at a liquid–liquid interface the waste powder increases the efficiency of H_2O_2 generation by ca. 20 times.

1. Introduction

The oxygen reduction reaction (ORR) is one of the most important reactions related to chemical energy conversion and storage [1]. 2-electron ORR produces H_2O_2 and can be employed for the sustainable generation of this chemical [2]. There is a strong demand for H_2O_2, because of its oxidative and bleaching properties. It is regarded as a versatile green oxidant and is commonly used in organic chemistry [3]. H_2O_2 is also widely used as an active component of disinfectants and antiseptics and as an agent for the removal of tastes and odours from water [4–6]. Recently its application as a fuel and oxidant in fuel cells has been demonstrated [7–9]. On a commercial scale, H_2O_2 is produced via the environmentally hazardous anthraquinone method [10].

By contrast, carbon-free methods like electrochemical ORR [1] are environmentally friendly. Electrons can be delivered from an external voltage source [11], via photocatalytic oxidation of various hole scavengers [12,13], or both [14]. ORR is thermodynamically favourable in a non-aqueous environment [15,16] and produces H_2O_2 in an acidified organic solvent [17,18], or at the liquid–liquid interface formed by an organic solvent and an acidic aqueous solution [16,19]. In the latter case, a sacrificial electron donor from the organic phase reduces oxygen in the presence of protons from the aqueous phase. ORR [20] and other biphasic reactions such as interfacial electron transfer [21,22], hydrogen evolution [23,24] and water oxidation [25] are accelerated by conductive nanoparticles generated/assembled at a liquid–liquid interface providing numerous electron paths. Here we will demonstrate that leached lithium battery (LiB) waste powder can be employed to increase the efficiency of H_2O_2 generation in a biphasic system, namely at liquid–liquid and electrode–electrolyte interfaces.

The LiB waste is obtained as a by-product when processing the electrodes of lithium batteries to recover lithium and transition metals [26–28]. As the waste consists of carbon and traces of cobalt, it seems to be a good candidate for a 2-electron ORR (electro)catalyst [29,30]. Here we show that LiB waste leached with acids for selective removal of metals can be assembled at the liquid–liquid interface formed by α,α,α-toluene (TFT) and an acidic aqueous solution. TFT can be used instead of the 1,2-dichloroethane [31,32] earlier proposed for biphasic H_2O_2 generation [19]. The progress of the reaction was monitored by colorimetry, UV–vis spectroscopy and scanning electrochemical microscopy (SECM). Additionally, we show that the same material deposited

* Corresponding authors.
E-mail addresses: mwarczak@ichf.edu.pl (M. Warczak), mopallo@ichf.edu.pl (M. Opallo).

https://doi.org/10.1016/j.elecom.2022.107239
Received 17 January 2022; Received in revised form 2 February 2022; Accepted 2 February 2022
Available online 5 February 2022

on an electrode surface promotes 2-electron ORR in an acidic aqueous solution with a significant decrease in overpotential.

2. Materials and methods

2.1. Materials

H_2SO_4 (96%, analytical grade) and H_2O_2 (30%, analytical grade) were purchased from STANLAB. TFT (≥99 %), $HClO_4$ (ACS reagent, 70%), a Nafion 117-containing solution (~5% in a mixture of lower aliphatic alcohols and water) and starch were supplied by Sigma Aldrich. Decamethylferrocene (DMFc) (99%) was obtained from ABCR GmbH & Co KG. KI (p.a.) was purchased from POCh. Argon and oxygen gases were supplied by MULTAX S.C. Deionized water with a resistivity of 18.2 MΩ·cm (Arium® Comfort Lab Water System, Sartorius) was used to prepare all solutions.

2.2. Methods

Images of the LiB powder were obtained using a scanning electron microscope (SEM) – FE-SEM Merlin (Zeiss) equipped with a Gemini II column working in a low kV value range (0.5–1.5 kV) with a low probe current (10–20 μA). The chemical composition of this material was examined using X-ray photoelectron spectroscopy (XPS) with a Microlab 350 (Thermo Electron) using AlKα non-monochromatic radiation (1486.6 eV) as a source, with a maximum resolution of 0.83 eV. UV–vis absorption spectra of the organic and aqueous phases were recorded using a Perkin Elmer Lambda 35 spectrophotometer.

Spent lithium-ion batteries were collected from laptops of various brands, including Samsung, Toshiba, Lenovo, and Hewlett-Packard. The electrodes were separated manually (10 g of dry mass washed with water) and treated with reducing and leaching agents (30% H_2O_2 solution in 1.5 M aqueous H_2SO_4) [27]. The post-leaching LiB waste powder was then washed with deionized water, dried and ground to homogenize it.

SECM and voltammetry were performed with an Ivium Bipotentiostat (Ivium Technologies, Netherlands) using a three-electrode system. In the SECM experiments, Pt microelectrodes (ca. 25 μm diameter, Goodfellow, England) immersed in the aqueous phase were used as a SECM probe, while a silver wire served as a pseudo-reference electrode to avoid the contribution of chloride ion oxidation to the measured current. For the voltammetric experiments, a glassy carbon (GC) disc (0.00785 cm^2) working electrode was covered by LiB powder in a Nafion film, prepared by dropping 1.5 μL of a powder dispersion of 5 mg in 10 μL of 5 % Nafion solution. Rotating disc electrode (RDE, Radiometer Analytical) voltammetry was performed on larger (0.07 cm^2) modified GC electrodes at various rotation speeds. Ag|AgCl|KCl 3 M was used as the reference electrode. In all experiments, a Pt wire served as the counter electrode.

All experiments were performed at room temperature.

3. Results and discussion

The SEM images of LiB powder reveal its heterogeneous granular structure (Fig. 1). On a solid surface these granules (50–100 nm) agglomerate to form irregularly sized and shaped clusters of greater size, up to 10 μm.

Analysis of the XPS spectra (Fig. S1 in the Supplemental file) shows that carbon (76%) and oxygen (16.5%) are the main components of the LiB powder. It also contains nitrogen (0.3%), phosphorus (0.3%) and fluorine (2.0%), from the $LiPF_6$ electrolyte and the products of its decomposition. Sulphur (4.2%) comes from the H_2SO_4 used for leaching and cobalt (0.6%) is the only metal left in measurable amounts.

The electrocatalytic properties of LiB powder towards the ORR were studied on two different supports: immobilized in the ionomer matrix on a glassy carbon (GC) electrode, and floating at the liquid–liquid interface. Both the electrode and the organic phase were in contact with the same acidic aqueous electrolyte. The cyclic voltammetry experiments with a LiB powder-modified GC electrode were performed in deoxygenated (after 1 h of purging with Ar) and oxygenated (after 30 min of purging with O_2) conditions in a sealed electrochemical cell (Fig. 2a).

The onset potential of the cathodic current seen in the O_2-saturated electrolyte indicates a ca. 0.3 V decrease in ORR overpotential when using LiB waste powder, compared with the bare GC electrode (the vertical blue dashed line in Fig. 2a shows the ORR onset potential). The shape of the cathodic wave with plateau currents indicates a lack of O_2 depletion adjacent to the catalyst. The value of the current density (-0.4 to −0.5 mA cm^{-2}) indicates a large modified electrode surface. The Tafel slope is quite high, ca. 100 mV higher than seen on platinum in the same electrolyte [33]. No significant HER overpotential decrease is seen in the absence of O_2. Two other effects are seen on CV curves recorded on modified electrodes. The capacitive current in a potential region where no faradaic reaction occurs is 10 times higher than that recorded on GC electrodes, indicating a significant enlargement of the conductive surface by LiB waste deposition. Also, at a potential above 0.4 V, a reversible redox couple is seen, which can be ascribed to the $Co^{2+/3+}$ redox couple [34].

To evaluate the kinetics of ORR on LiB powder-modified electrodes, voltammetric experiments were conducted using a RDE (Fig. 2c). The number of transferred electrons (n) per O_2 molecule was calculated according to the Koutecký−Levich equation [35]:

$$\frac{1}{i} = \frac{1}{i_k} + \frac{1}{B}\omega^{-1/2} \quad (1)$$

$$B = 0.62nFAD^{2/3}\vartheta^{-1/6}C_{ox} \quad (2)$$

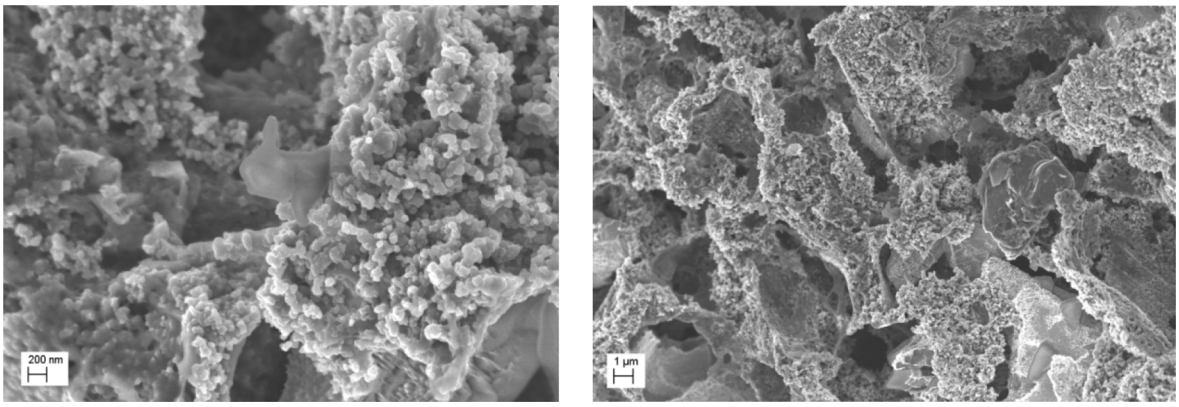

Fig. 1. SEM images of post-leaching waste LiB powder (different magnifications).

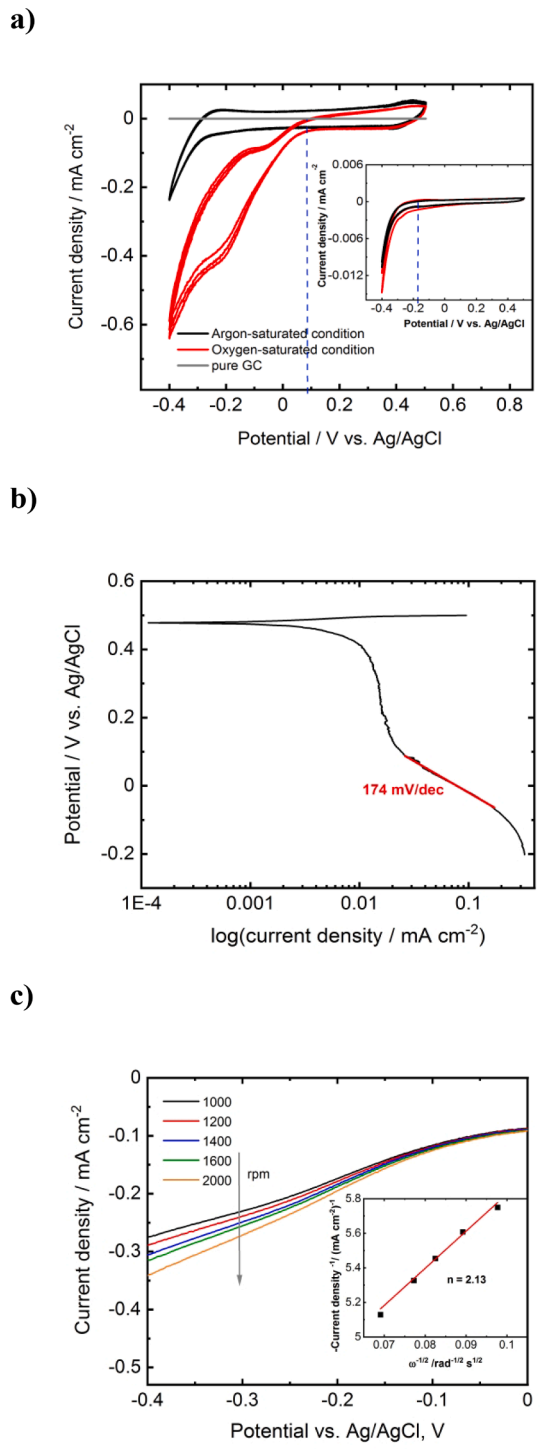

Fig. 2. (a) Cyclic voltammograms recorded with a bare GC (grey curve and inset) and with a GC modified with LiB powder in O_2-saturated (red) and Ar-saturated (black) aqueous 0.1 M $HClO_4$, scan rate: 5 mV s^{-1}; vertical blue dashed line – ORR onset potential (b) Tafel plot obtained from voltammograms recorded with a LiB waste-modified electrode at 1 mV s^{-1} in an O_2-saturated electrolyte; (c) Linear sweep voltammograms recorded for LiB powder-modified GC RDE at various rpm values in O_2-saturated 0.1 M $HClO_4$ with a scan rate of 20 mV s^{-1} and the corresponding Koutecký-Levich plot of the currents at −0.2 V vs. Ag/AgCl electrode (inset). (For interpretation of the references to colour in this figure legend, the reader is referred to the web version of this article.)

from the current (i) at −0.2 V, where i_k is the kinetic current, ω is the electrode rotation rate (rad s^{-1}), F is the Faraday constant (96 485C mol^{-1}), A is the electrode area (0.07 cm^2), D is the diffusion coefficient (1.9×10^{-5} cm^2 s^{-1} for O_2 in 0.1 M $HClO_4$ [36]), ν is the kinematic viscosity (0.01 m^2 s^{-1} for 0.1 M $HClO_4$ [36]), and C_{ox} is O_2 concentration (1.2×10^{-3} mol L^{-1} in 0.1 M $HClO_4$ [36]) at 298 K. From the slope of the K-L plot, it can be concluded that ORR at the LiB waste follows a 2-electron path and H_2O_2 is generated.

Having established the electrocatalytic activity of LiB waste powder towards the ORR, experiments were conducted in the biphasic system. When 5 mM DMFc solution in TFT (2 mL) was injected to the bottom of a flask containing an aqueous (2 mL of 0.1 M $HClO_4$) suspension of LiB powder (1 mg mL^{-1}), a nanostructured material sedimented at the liquid|liquid interface (Fig. 3a, b). In the absence of LiB waste powder almost no change in the colour of the organic phase was observed within 3.5 h, whereas in the presence of this material, the TFT solution turned green, indicating the formation of blue $DMFc^+$ cations (Fig. 3a, b). This is confirmed by the decrease in the absorption band at λ = 425 nm and the appearance of an absorption band at λ = 779 nm, together with the appearance of shoulders at a lower wavelength in the UV–vis spectrum (Fig. 3c) [19]. These changes are significant only in the presence of LiB waste powder. After adding KI and starch, a sample of the aqueous phase collected from the reactor with post-leaching LiB powder turned violet: a colour characteristic of a starch-I_3^- complex, an indicator of H_2O_2 generation [32]. This was confirmed by the appearance of an absorption peak at λ = 330 nm in the UV–vis spectrum, characteristic of triiodide (Fig. 3d).

The above results and earlier findings [37] indicate that the studied reaction can be described as follows:

$$2DMFc_{(TFT)} + 2H^+_{(aq)} + O_2 + 2ClO_4^-{}_{(aq)} \rightarrow 2DMFc^+_{(TFT)} + H_2O_{2\,(aq)} + 2ClO_4^-{}_{(TFT)} \quad (3)$$

Clearly, the presence of LiB waste assembled at the interface accelerates this reaction. In order to quantitatively estimate the catalytic effect of LiB waste, the efficiency of H_2O_2 generation was estimated by SECM. Cyclic voltammograms were recorded as the SECM tip approached the liquid–liquid interface in 20 μm steps in the potential range from −0.4 V to 1.4 V vs. the Ag-wire quasi-reference electrode at a scan rate of 100 mV s^{-1}. This procedure was applied to avoid the gradual loss of Pt activity towards oxidation of H_2O_2 [38]. The anodic current at potentials above 0.8 V corresponds to H_2O_2 electrooxidation and is larger when the SECM tip approaches the liquid–liquid interface (Fig. 4a). Approach curves were constructed from the values of the diffusion limiting current (i) at 0.9 V at every vertical position of the SECM tip. From these values, local H_2O_2 concentrations ($c(H_2O_2)$) were calculated:

$$c(H_2O_2) = \frac{i}{(4nFDr)} \quad (4)$$

where F is the Faraday constant, r is the radius of the microelectrode (11.42 μm), D is the diffusion coefficient of H_2O_2 (8.8×10^{-6} cm^2 s^{-1}) [39] and n is the number of electrons transferred per analyte molecule (2).

As the SECM tip approaches the liquid–liquid interface $c(H_2O_2)$ increases and its value is significantly larger in the presence of the assembled LiB waste powder (Fig. 4b): The flux of H_2O_2 (J_{H2O2}) calculated from the slope of the approach curve (0.11 nmol cm^{-2} s^{-1}) is ca. 20 times higher than that at the bare interface (5.5 pmol cm^{-2} s^{-1}) (Fig. 4b).

4. Conclusions

We have demonstrated that post-leaching LiB powder assembles at the liquid–liquid interface and exhibits catalytic properties towards 2-electron ORR in the presence of the strong electron donor DMFc in the

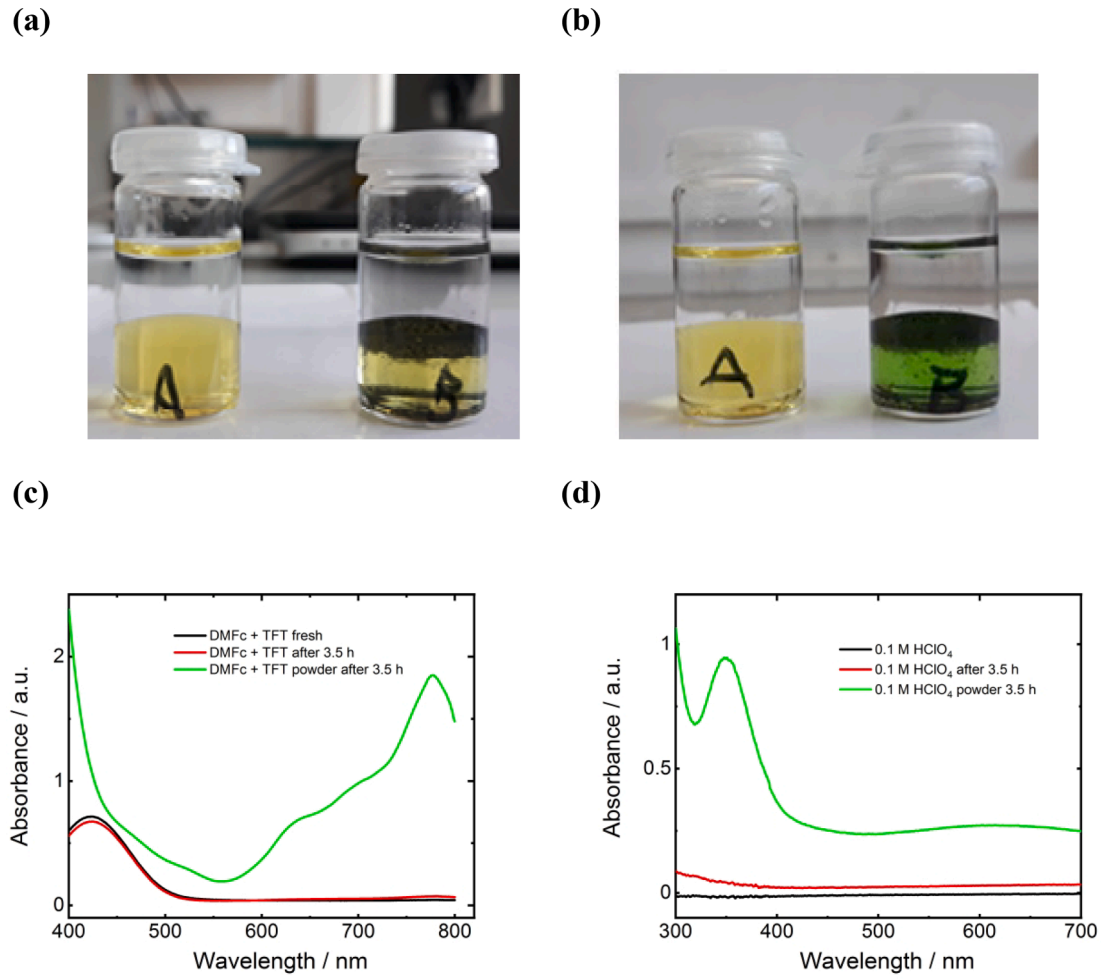

Fig. 3. Results of flask experiments (see text for details): (a) freshly prepared; (b) after 3.5 h. The bottom (organic) phase consisted of 5 mM DMFc in TFT and the upper (aqueous) phase consisted of 0.1 M $HClO_4$. UV–vis spectra of (c) the organic phase and (d) the aqueous phase after the reaction and addition of KI and starch.

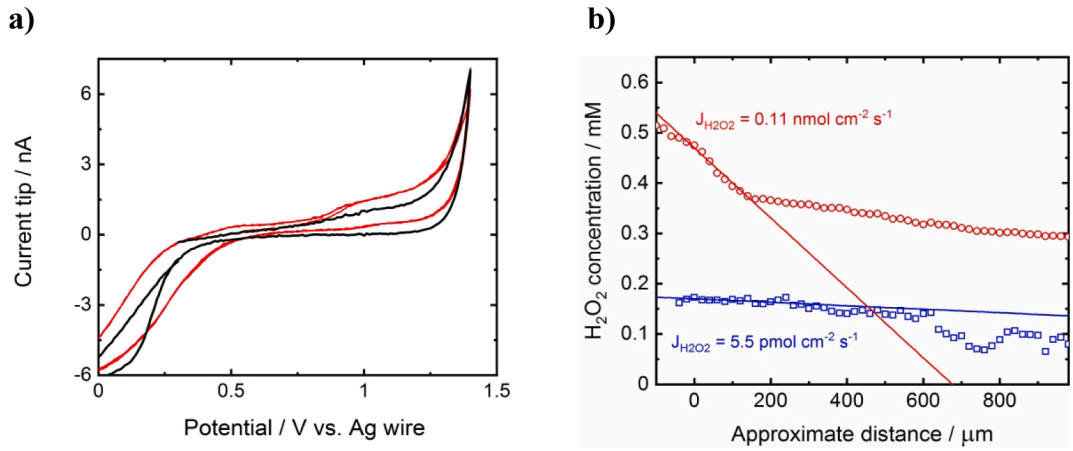

Fig. 4. (a) Examples of cyclic voltammograms recorded as the SECM Pt tip approaches the liquid–liquid interface in 20 µm steps with a scan rate of 100 mV s^{-1}. The red curve was recorded closer to the liquid–liquid interface than the black one (b) SECM approach curves recorded in the presence (red curve) and absence (blue curve) of LiB powder in the 5 mM DMFc in TFT/0.1 M $HClO_4$ biphasic system. The SECM experiments were conducted 15 min after mixing the organic and aqueous phases in both cases (with and without LiB waste powder). (For interpretation of the references to colour in this figure legend, the reader is referred to the web version of this article.)

organic phase. This indicates that not only noble metal nanoparticles catalyse this reaction [22]. Also, the data obtained with LiB powder-modified electrodes indicate 2-electron ORR stoichiometry and a significant decrease in the overpotential versus glassy carbon in acidic solution. At the moment, it is unclear whether this catalytic effect results from the presence of carbon as the main component of LiB waste and/or cobalt oxide. Both materials are known to catalyse 2-electron ORR [29,30]. These results demonstrate a prospective use for the waste left

after transition metal recovery from lithium battery electrodes. Studies of the application of these materials for ORR in alkaline solution, and of the effect of LiB composition, especially the nature of the carbonaceous material, are underway.

CRediT authorship contribution statement

Magdalena Warczak: Conceptualization, Methodology, Validation, Formal analysis, Investigation, Resources, Data curation, Writing – original draft, Writing – review & editing, Visualization, Supervision. **Magdalena Osial:** Methodology, Validation, Investigation, Resources, Writing – review & editing, Visualization. **Weronika Urbanska:** Methodology, Validation, Investigation, Resources, Writing – review & editing. **Marcin Pisarek:** Methodology, Validation, Formal analysis, Investigation, Resources, Writing – review & editing. **Wojciech Nogala:** Methodology, Validation, Formal analysis, Investigation, Resources, Data curation, Writing – review & editing. **Marcin Opallo:** Conceptualization, Methodology, Validation, Writing – original draft, Writing – review & editing, Supervision, Project administration, Funding acquisition.

Declaration of Competing Interest

The authors declare that they have no known competing financial interests or personal relationships that could have appeared to influence the work reported in this paper.

Acknowledgements

This work was financially supported by the National Science Centre (NCN, Poland) through grant UNISONO Solar-Driven Chemistry No. 2019/01/Y/ST4/00022.

Appendix A. Supplementary data

Supplementary data to this article can be found online at https://doi.org/10.1016/j.elecom.2022.107239.

References

[1] M.L. Pegis, C.F. Wise, D.J. Martin, J.M. Mayer, Oxygen reduction by homogeneous molecular catalysts and electrocatalysts, Chem. Rev. 118 (5) (2018) 2340–2391, https://doi.org/10.1021/acs.chemrev.7b00542.
[2] R.S. Disselkamp, Energy storage using aqueous hydrogen peroxide, Energy Fuels 22 (4) (2008) 2771–2774, https://doi.org/10.1021/ef800050t.
[3] H. Targhan, P. Evans, K. Bahrami, A review of the role of hydrogen peroxide in organic transformations, J. Ind. Eng. Chem. 104 (2021) 295–332, https://doi.org/10.1016/j.jiec.2021.08.024.
[4] J.P. Duguet, E. Brodard, B. Dussert, J. Mallevialle, Improvement in the effectiveness of ozonation of drinking water through the use of hydrogen peroxide, Ozone Sci. & Eng. 7 (3) (1985) 241–258, https://doi.org/10.1080/01919518508552366.
[5] Y. Wang, J. Yu, D. Zhang, M. Yang, Addition of hydrogen peroxide for the simultaneous control of bromate and odor during advanced drinking water treatment using ozone, J. Environ. Sci. 26 (3) (2014) 550–554, https://doi.org/10.1016/S1001-0742(13)60409-X.
[6] Y.C. Jin, Y.J. Shi, Z.Y. Chen, R.Y. Chen, X. Chen, X. Zheng, Y.X. Liu, Combination of sunlight with hydrogen peroxide generated at a modified reticulated vitreous carbon for drinking water disinfection, J. Clean. Product. 252 (2020), https://doi.org/10.1016/j.jclepro.2019.119794.
[7] Y. Yamada, S. Yoshida, T. Honda, S. Fukuzumi, Protonated iron–phthalocyanine complex used for cathode material of a hydrogen peroxide fuel cell operated under acidic conditions, Energy Environ. Sci. 4 (2011) 2822–2825, https://doi.org/10.1039/C1EE01587G.
[8] E. Miglbauer, P.J. Wojcik, E.D. Glowacki, Single-compartment hydrogen peroxide fuel cells with poly(3,4-ethylenedioxythiophene) cathodes, Chem. Commun. 54 (2018) 11873, https://doi.org/10.1039/C8CC06802J.
[9] J. Ji, I. Chung, J. Kwon, The effect of a vitamin B12 based catalyst on hydrogen peroxide oxidation reactions and the performance evaluation of a membraneless hydrogen peroxide fuel cell under physiological pH conditions, J. Mater. Chem. C 8 (2020) 2749–2755, https://doi.org/10.1039/C9TC06345E.
[10] H. Reild, G. Pfleiderer, Production of hydrogen peroxide, Patent US2158525 A, Ig Farbenindustrie AG, 1939.
[11] M. Warczak, M. Gryszel, M. Jakešová, V. Đerek, E.D. Głowacki, Organic semiconductor perylenetetracarboxylic diimide (PTCDI) electrodes for electrocatalytic reduction of oxygen to hydrogen peroxide, Chem. Commun. 54 (16) (2018) 1960–1963, https://doi.org/10.1039/C7CC08471D.
[12] K. Mase, M. Yoneda, Y. Yamada, S. Fukuzumi, Efficient photocatalytic production of hydrogen peroxide from water and dioxygen with bismuth vanadate and a cobalt (II) chlorin complex, ACS Energy Lett. 1 (2016) 913–919, https://doi.org/10.1021/acsenergylett.6b00415.
[13] Z. Liu, X. Sheng, D. Wang, X. Feng, Efficient hydrogen peroxide generation utilizing photocatalytic oxygen reduction at a triphase interface, iScience 17 (2019) 67–73, https://doi.org/10.1016/j.isci.2019.06.023.
[14] M. Gryszel, A. Markov, M. Vagin, E.D. Głowacki, Organic heterojunction photocathodes for optimized photoelectrochemical hydrogen peroxide production, J. Mater. Chem. A 6 (48) (2018) 24709–24716, https://doi.org/10.1039/C8TA08151D.
[15] S. Fukuzumi, S. Mochizuki, T. Tanaka, Metalloporphyrin-catalyzed reduction of dioxygen by ferrocene derivatives, Chem. Lett. 18 (1) (1989) 27–30, https://doi.org/10.1246/cl.1989.27.
[16] M.A. Mendez, R. Partovi-Nia, I. Hatay, B. Su, P.Y. Ge, A. Olaya, N. Younan, M. Hojeij, H.H. Girault, Molecular electrocatalysis at soft interfaces, Phys. Chem. Chem. Phys. 12 (2010) 15163–15171, https://doi.org/10.1039/C0CP00590H.
[17] R. Prins, A.G.T.G. Kortbeek, Electron spin resonance spectra of ferricenium salts, J. Organomet. Chem. 33 (1971) C33–C34, https://doi.org/10.1016/S0022-328X(00)88390-4.
[18] B. Su, I. Hatay, P.Y. Ge, M. Mendez, C. Corminboeuf, Z. Samec, M. Ersoz, H. H. Girault, Oxygen and proton reduction by decamethylferrocene in non-aqueous acidic media, Chem. Commun. 46 (2010) 2918–2919, https://doi.org/10.1039/B926963K.
[19] B. Su, R. Partovi-Nia, F. Li, M. Hojeij, M. Prudent, C. Corminboeuf, Z. Samec, H. Girault, H2O2 generation by decamethylferrocene at a liquid|liquid interface, Angew. Chem. Int. Ed. 47 (2008) 4675–4678, https://doi.org/10.1002/anie.200801004.
[20] E. Smirnov, P. Peljo, M.D. Scanlon, H.H. Girault, Gold nanofilm redox catalysis for oxygen reduction at soft interfaces, Electrochim. Acta 197 (2016) 362–373, https://doi.org/10.1016/j.electacta.2015.10.104.
[21] E. Smirnov, P. Peljo, M.D. Scanlon, H.H. Girault, Interfacial redox ratalysis on gold nanofilms at soft interfaces, ACS Nano 9 (2015) 6565–6575, https://doi.org/10.1021/acsnano.5b02547.
[22] M.D. Scanlon, E. Smirnov, T.J. Stockmann, P. Peljo, Gold nanofilms at liquid–liquid interfaces: an emerging platform for redox electrocatalysis, nanoplasmonic sensors, and electrovariable optics, Chem. Rev. 118 (2018) 3722–3751, https://doi.org/10.1021/acs.chemrev.7b00595.
[23] I. Hatay, B. Su, F. Li, R. Partovi-Nia, H. Vrubel, X.L. Hu, M. Ersoz, H.H. Girault, Hydrogen evolution at liquid–liquid interface, Angew. Chem. Int. Ed. 48 (2009) 5139–5142, https://doi.org/10.1002/anie.200901757.
[24] F. Ozel, E. Aslan, E.M. Sarilmaz, I.H. Patay, Hydrogen evolution catalyzed by Cu2WS4 at liquid–liquid interfaces, ACS Mater. Interfaces 8 (2016) 25881–25887, https://doi.org/10.1021/acsami.6b05582.
[25] S. Rastgar, M. Pilarski, G. Wittstock, A polarized liquid–liquid interface meets visible light-driven catalytic water oxidation, Chem. Comm. 52 (76) (2016) 11382–11385, https://doi.org/10.1039/C6CC04275A.
[26] X. Yang, Y. Zhang, Q.i. Meng, P. Dong, P. Ning, Q. Li, Recovery of valuable metals from mixed spent lithium-ion batteries by multi-step directional precipitation, RSC Adv. 11 (1) (2021) 268–277, https://doi.org/10.1039/D0RA09297E.
[27] W. Urbanska, M. Osial, Investigation of the physico-chemical properties of the products obtained after mixed organic-inorganic leaching of spent Li-ion batteries, Energies 13 (2020) 6732, https://doi.org/10.3390/en13246732.
[28] L.-F. Zhou, D. Yang, T. Du, H. Gong, W.-B. Luo, The current process for the recycling of spent lithium ion batteries, Front. Chem. 8 (2020), 578044, https://doi.org/10.3389/fchem.2020.578044.
[29] M. Campos, W. Siriwatcharapiboon, R.J. Potter, S.L. Horswell, Selectivity of cobalt-based catalysts towards hydrogen peroxide formation during the reduction of oxygen, Catal. Today 202 (2013) 135–143, https://doi.org/10.1016/j.cattod.2012.05.015.
[30] N. Daems, X. Sheng, I.F.J. Vankelecom, P.P. Pescarmona, Metal-free doped carbon materials as electrocatalysts for the oxygen reduction reaction, J. Mater. Chem. A 2 (12) (2014) 4085–4110, https://doi.org/10.1039/C3TA14043A.
[31] W. Adamiak, J. Jedraszko, O. Krysiak, W. Nogala, J.C. Hidalgo-Acosta, H. H. Girault, M. Opallo, Hydrogen and hydrogen peroxide formation in trifluorotoluene-water biphasic systems, J. Phys. Chem. C 118 (2014) 23154–23161, https://doi.org/10.1021/jp507310d.
[32] W. Adamiak, J. Jedraszko, W. Nogala, M. Jönsson-Niedziolka, S. Dongmo, G. Wittstock, H.H. Girault, M. Opallo, A simple liquid–liquid biphasic system for hydrogen peroxide generation, J. Phys. Chem. C 119 (34) (2015) 20011–20015, https://doi.org/10.1021/acs.jpcc.5b06620.
[33] N.M. Marković, H.A. Gasteiger, B.N. Grgur, P.N. Ross, Oxygen reduction reaction on Pt(111): effects of bromide, J. Electroanal. Chem. 467 (1-2) (1999) 157–163, https://doi.org/10.1016/S0022-0728(99)00020-0.
[34] L. Ma, S.-F. Hung, L. Zhang, W. Cai, H.B. Yang, H.M. Chen, B. Liu, High spin state promotes water oxidation catalysis at neutral pH in spinel cobalt oxide, Ind. Eng. Chem. Res. 57 (5) (2018) 1441–1445, https://doi.org/10.1021/acs.iecr.7b04812.
[35] A.J. Bard, L.R. Faulkner, Electrochemical Methods: Fundamentals and Applications, 2nd ed., J. Wiley and Sons, New York, 2001, p. 341.
[36] M. Yang, H. Chen, D. Yang, Y. Gao, H. Li, High-performance electrocatalyst for oxygen reduction reaction derived from copolymer networks and iron(ii) acetate, RSC Adv. 6 (2016) 97259–97265, https://doi.org/10.1039/C6RA24314B.

[37] J. Jedraszko, O. Krysiak, W. Adamiak, W. Nogala, H.H. Girault, M.W. Opallo, H2O2 generation at carbon paste electrode with decamethylferrocene solution in 2-nitrophenyloctyl ether as a binder. Catalytic effect of MoS2 particles, ChemElectroChem 3 (2016) 1400–1406, https://doi.org/10.1002/celc.201600242.

[38] S.A.G. Evans, J.M. Elliott, L.M. Andrews, P.N. Bartlett, P.J. Doyle, G. Denuault, Detection of hydrogen peroxide at mesoporous platinum microelectrodes, Anal. Chem. 74 (6) (2002) 1322–1326, https://doi.org/10.1021/ac011052p.

[39] M.A. Komkova, A. Pasquarelli, E.A. Angreev, A.A. Galushin, A.A. Karyakin, Prussian blue modified boron-doped diamond interfaces for advances H2O2 electrochemical sensors, Electrochim. Acta 339 (2020), https://doi.org/10.1016/j.electacta.2020.135924.